

Arguments_For_The_Physical_Nature_of_the_Triggered_Ion-acoustic_Waves_Observed_On_The_Parker_Solar_Probe

By Forrest Mozer¹, Stuart Bale¹, Paul.Kellogg³, Orlando Romeo², Ivan Vasko², and Jaye Verniero⁴

1. Physics Department and Space Sciences Laboratory, University of California, Berkeley,94720
2. Space Sciences Laboratory, University of California, Berkeley,94720
3. University of Minnesota, Minneapolis, Minnesota, 55455
4. Goddard Space Flight Center, Greenbelt,Md., 20706

Corresponding author: Forrest.Mozer@gmail.com

Triggered ion-acoustic waves are a pair of coupled waves observed in the previously unexplored plasma regime near the Sun. They may be capable of producing important effects on the solar wind. Because this wave mode has not been observed or studied previously and it is not fully understood, the issue of whether it has a natural origin or is an instrumental artifact can be raised. This paper discusses this issue by examining 13 features of the data such as whether the triggered ion-acoustic waves are electrostatic, whether they are both narrow-band, whether they satisfy the requirement that the electric field is parallel to the k-vector, whether the phase difference between the electric field and the density fluctuations is 90 degrees, whether the two waves have the same phase velocity as they must if they are coupled, whether the phase velocity is that of an ion-acoustic wave, whether they are associated with other parameters such as electron heating, whether the electric field instrument otherwise performed as expected, etc. The conclusion reached from these analyses is that triggered ion-acoustic waves are highly likely to have a natural origin although the possibility that they are artifacts unrelated to processes occurring in the natural plasma cannot be eliminated. This inability to absolutely rule out artifacts as the source of a measured result is a characteristic of all measurements.

I SUMMARY OF TRIGGERED ION-ACOUSTIC WAVE PROPERTIES

The Parker Solar Probe has measured triggered ion-acoustic waves (TIAW) in each of the seven orbits that passed through the altitude range of 15-25 solar radii. Earlier papers [Mozer et al, 2021; 2022a] have offered detail descriptions and discussions of their properties. In summary, they have the following properties:

- A pair of coupled waves, one of which is at a frequency of a few Hertz and the other is at few hundred Hertz
- The two waves are coupled such that the high frequency wave sometimes occurs in short bursts during successive periods of the low frequency sine wave and at a fixed phase of this lower frequency wave.
- The waves are electrostatic.
- Both the high and the low frequency waves are narrow band, effectively pure sine waves.
- They can exist as a pair for times as long as several hours.
- They are associated with heating the core electron distribution.

The Parker Solar Probe is in a solar orbit with one surface (the heat shield) facing the Sun near perihelion. The line of sight from the spacecraft to the Sun is the spacecraft Z-direction, along which the typical magnetic field and solar wind flow are oriented near perihelion. The X-Y plane, perpendicular to the Sun-satellite line, contains a two-component electric field and spacecraft potential measurement by antennas that are not much larger than the spacecraft [Bale et al, 2016]. By fitting the measured spacecraft potential to the low-rate density measurements obtained from the SWEAP plasma measurements [Kasper et al, 2016; Whittlesey et al, 2020], higher frequency estimates of the plasma density and density fluctuations are obtained [Mozer et al, 2022b]. In addition, the SWEAP/SPAN-I [Livi et al, 2022] instrument provided the solar wind velocity utilized in the following analyses. The solar wind speed, magnetic field, plasma density, ion temperature and other parameters for the event that follows are given in Table 1. All data presented in this paper are in the spacecraft coordinates whose X, Y, and Z directions are defined above.

Figure 1 presents TIAW observed on January 19, 2021. The four pairs of panels each display EX and the density fluctuations, $\delta n/n$. Panel (1a), gives 1 Hz high pass filtered electric field data that illustrates the low and high frequency waves that are phase locked such that the high frequency bursts occur at fixed phases of the low frequency signal. Panel (1b) illustrates the density fluctuations measured above 1 Hz and they show mainly the low frequency wave signal. Panels (1d) and (1e) show the low frequency (0.5-2 Hz) components of the TIAW with $\delta E \sim 0.5$ mV/m and $\delta n/n \sim 0.13$, while panels (1f) and (1g) illustrate the high frequency (>100 Hz) components having $\delta E \sim 4$ mV/m and $\delta n/n \sim 0.004$. Panels (h) and (i) present a short portion of the high frequency components to illustrate that they are nearly pure sine waves, (the full spectral width at half-maximum is less than 60 Hz) which is not expected because only broad band waves have been observed earlier [Gurnett and Anderson, 1977; Gurnett and Frank, 1978; Kurth et al, 1979; Hull et al., 2006; Mozer et al, 2020; Vasko et al., 2022]. Figure 1 presents the same event as that described in Figure 6 of Mozer et al [2021] and it was selected to benefit from this earlier information that shows the phase locking of the low and high frequency waves and the absence of a magnetic field signature during such events. It is important to note that the potentials of antennas 1 through 4 produced both the electric field and the density data because the difference between potential pairs is the electric field and the sum of the four potentials is the spacecraft potential that gives the plasma density [Mozer et al, 2022b]. Thus, although the origins of the electric field and density are related, they are really two different quantities.

II ARGUMENTS CONCERNING WHETHER TRIGGERED ION-ACOUSTIC WAVES ARE A NATURAL PHYSICAL PHENOMENON OR AN INSTRUMENTAL ARTIFACT.

IIa The TIAW occur at times of elevated electron temperature in the solar wind. Most importantly, in the absence of TIAW, electrons are not heated at 20-25 solar radii.

Triggered ion-acoustic waves are seen at 20-25 solar radii on practically every orbit where they have been searched for. Mozer et al [2022a] showed this to be true for orbits 6, 7, 8, and 9, and more recent observations on orbits 10, 11, and 12 also confirm their presence. The core electron temperature has been observed to increase in conjunction with all triggered ion-acoustic wave events [Mozer et al, 2022a] and, most importantly, such heating is absent when there are no triggered waves [see Figure 1 of Mozer et al, 2022a]. This correlation may exist because core

electrons are heated by the triggered ion-acoustic waves or, conversely, because the increased electron temperature is favorable for generation of TIAWs.

Other non-wave electron heating mechanisms may also operate in the solar wind. For example, Boldyrev et al [2020] proposed that, due to conservation of their magnetic moments, solar wind electrons form a beam collimated along the magnetic-field lines. Due to weak energy exchange with the background plasma, the beam population slowly loses its energy and heats the background plasma. In this model, electrons are heated more or less uniformly as a function of distance while the observed heating largely occurs between 20 and 25 solar radii [Mozer et al, 2022a] and only when TIAW are present.

The amplitudes, $\delta\phi$, of the electrostatic potential of both TIAW waves can be estimated in the following way. Because the observed waves are expected to have phase speeds much smaller than the electron thermal speed, the parallel electric field should be balanced by the electron pressure gradient [Davidson, 1972; Kelley and Mozer, 1972]

$$enE_{\parallel} = -\nabla_{\parallel}p_e \quad (1)$$

where n is the plasma density, and $\nabla_{\parallel}p_e$ is the parallel electron pressure gradient, $\nabla_{\parallel}nkT_e$. Thus, $\delta\phi/T_e \approx \delta n/n$. With the local electron temperature for the interval in Figure 1 of about 54 eV being constant on the time scale of the waves (Table 1), we find for the high and low frequency pressure gradients that

$$\delta\phi_h \approx 0.2 \text{ V} \quad \text{and} \quad \delta\phi_l \approx 7 \text{ V} \quad (2)$$

Since ion-acoustic waves have speeds much slower than the electron thermal speed, the electron heating due to their interaction with these waves via the Landau resonance can only be less than or the order of their potentials. Thus, the direct electron heating due to the high-frequency waves cannot exceed 1%, while the direct heating due to the low-frequency waves can be as large as 10%. This amount of heating is generally consistent with the core electron temperature increases that have been observed at the times of these waves [Mozer et al, 2022a].

IIb The high and the low frequency waves are both electrostatic because they have density fluctuations and no magnetic field component.

Panels (b) and (c) of Figure 1 of Mozer et al, [2021] show prominent signatures in the electric field spectra during a 20-hour interval containing the high frequency component of the triggered ion-acoustic wave that varied from 1000 to 200 Hz. Panels (e) and (f) of this figure [Mozer et al, 2021] cover the same time and frequency interval for two components of the magnetic field measured by the search coil magnetometer. Because there is no corresponding signal in the magnetic field data, there is no magnetic field in the high frequency wave. For a 100 km/sec phase velocity of these waves [Mozer et al, 2021], the magnetic field associated with a phase speed $E/B \sim 100$ km/sec in the presence of the ~ 1 mV/m low frequency electric field of Figure 1a, if it was an electromagnetic wave, would be ~ 10 nT. The upper limit to the observed magnetic field at this low wave frequency is at least an order of magnitude less, showing that the low frequency wave also does not have a magnetic component. Thus, the waves of interest must be electrostatic. These results are also

expected from Figure 1 which shows correlated electric field and density fluctuations in both the low and high frequency waves, as well as the magnetic field in panel (1c) which is a 3.3 Hz unrelated electromagnetic wave having no signal at the 1.3 Hz signal of the electrostatic TIAW wave.

IIc The electric field fluctuations in the high frequency wave are parallel to the k-vector in the X-Y plane, as they must be if the wave is real.

Figure 2 provides detailed information on the event of Figure 1 that enables a measurement of the angle between the electric field and the k-vector in the X-Y plane. As seen in panel (2a), the 600 Hz electric field oscillated in the $\pm X$ direction while the component of the solar wind velocity in the X-Y plane was in the $-X$ direction (panel 2c) and the magnetic field in the X-Y plane was inclined about 30° away from the $+X$ -axis (panel 2b). The direction of wave propagation may be determined from timing the crossing of the wave over each of the antennas. Panel (2d) shows that antennas V1 and V4 received the maximum wave signal at about the same time. From the geometry illustrated in Figure 3, this requires that the wave traveled in either the $+X$ or $-X$ direction. If it traveled in the $-X$ direction, the signals on V1 and V4 would precede the signals on V2 and V3, as actually happened in panel (2d). (The negatives of the signals on V2 and V3 are plotted to compensate for the fact that the peak of a wave traveling to the left produces negative voltages on V2 and V3 because they measure the voltage on the antenna minus the voltage of the spacecraft body). In summary, in the spacecraft X-Y plane, the wave propagated in the $-X$ direction and the electric field oscillations were along this direction. Thus, in the X-Y plane the requirement that E must be parallel to k is satisfied.

IIId The phase velocity of the high frequency wave is consistent with that of an ion-acoustic wave

The high frequency wave speed in the X-Y plane may be determined from the time lags of the single ended potentials in Figure (2d). The time difference between the wave reaching V1/V4 and V2/V3 was about 0.53 msec and the wave traveled about three meters during this time. Thus, in the spacecraft X-Y frame, the wave speed in the X direction was -6 km/sec. Because the solar wind speed in the X direction was -90 km/sec in panel (2c), the wave speed in the plasma frame was in the X direction at about -84 km/sec. Neither the electric field nor the wave speed in the Z direction were measured so the total phase velocity cannot be determined. However, from the measured wave speed in the X-Y plane, a total phase velocity that is consistent with an electrostatic wave is quite plausible because the ion acoustic phase velocity at this time was determined for $k\lambda_d < 1$ and $T_i/T_e > 1$ to be $(T_i/M_i)^{0.5} \sim 150$ km/sec.

IIe To be physical, the two TIAW must have the same phase velocity because they are coupled. Direct measurements of the phase velocities in the plasma frame show that they are equal in magnitude and direction in the X-Y plane to well within experimental uncertainties.

At a frequency of a few Hz there is both an electrostatic wave, as indicated by the density fluctuations in Figure (1b), and an electromagnetic wave, as indicated by the magnetic fluctuations of Figure (4c) and (4d). Spectral plots of the electric field cannot distinguish between these two

modes because they have power at similar frequencies. In panel (4a), the x-component of the filtered low frequency electric field appears to be a nearly pure sinusoid, which signifies that the electrostatic field was greater than the electromagnetic field for this component. By comparison, EY in panel (4b) deviates significantly from a sine wave. That this is because of the predominance of the y-component of the electromagnetic wave is seen by comparing EY with the similar wave form of BX in panel (4c). Thus, it is concluded that the low frequency electrostatic wave oscillated primarily in the x-direction.

Figure 5 presents the band pass filtered low frequency potentials on the four electric field antennas in panels (5a) through (5d). That the amplitudes of the signals and, to some extent, their frequencies vary within the bandwidth is due to the electromagnetic field contamination. Determining the time differences between these various voltage signals to obtain the low frequency phase velocity is less accurate for this reason as well as, for the reason that because of the low frequency of the wave, a short time difference is more difficult to determine than is the case for the high frequency wave of section IId. Nevertheless, the cross correlation of antenna pairs as a function of the lag time is presented in panel (5e) in order to obtain approximate information on the low frequency wave propagation direction and speed. That the time lags between signals on V2 and V3 (the red curve) as well as between signals on V1 and V4 (the green curve) are minimum suggests that the wave propagated in $\pm X$ direction, as did the high frequency wave. That the correlation between V1 and V2 (the black curve) is maximum for a lag of -2 milliseconds suggests both that the wave propagated in the $-X$ direction and that it propagated at a speed of about 2 km/sec. Thus, in the plasma frame, the low frequency wave traveled in the X -direction at about -88 km/sec. This velocity is consistent in magnitude and direction with the -84 km/sec speed of the high frequency wave. And thus, the low and high frequency waves traveled in the X - Y plane in the same direction and at the same phase velocity in the plasma frame, as they must in order to be coupled. It is noted that the near equality of the two phase speeds results from the fact that their phase speeds in the spacecraft frame were small, such that the exact values of the phase speeds in the spacecraft frame does not matter.

IIf The phase difference between the electric field and density fluctuations in the high frequency wave was 90 degrees, as must be the case for real electrostatic waves.

Because of equation (1), the electric field and the density fluctuations must be 90 degrees out of phase. As seen by the vertical dashed lines in Figure 1 panel (1h) and panel (1i), this requirement is fulfilled by the high frequency wave of the triggered ion-acoustic wave pair. Because of the presence of additional electric fields in electromagnetic waves at low frequencies, this requirement is hard to verify for the low frequency electrostatic wave although it is suggested by comparison of the plots in Figures (1d) and (1e).

IIfg The TIAW are observed to persist for up to several hours at a time. This result may be understood theoretically.

Normal ion-acoustic waves have shorter durations than do the TIAW [Kurth et al., 1979; Mozer et al., 2020]. Figure 5 of Mozer et al [2021] shows a continuous 30-minute segment of a TIAW that actually lasted for hours, as can be seen from the spectra of Figure 1 in that paper. Such waves appear when the ratio of the core electron to ion temperature, T_e/T_i , is greater than one, as seen in

Table 1 of this paper and Figures 1-4 of Mozer et al [2022a]. In such an environment, Landau damping is diminished. Additionally, if the waves are continuously driven by an unknown mechanism, their durations may be independent of the damping.

IIIh The high frequency wave in TIAW is narrow band. Such narrow band waves are not found in ordinary ion-acoustic waves. Formation of this wave by coupling with the low frequency wave can explain why the high frequency wave is narrow band.

Depending on the formation mechanism, an ion-acoustic wave may initially contain any number of discrete frequencies, n , where $n \geq 1$. The value $n=1$ is possible although previous observations in the solar wind [Kurth et al., 1979] and the Earth's bow shock [Hull et al., 2006; Vasko et al., 2022] showed that n is usually large because ion-acoustic waves typically have spectral widths comparable with the wave central frequency. Because the high frequency TIAW generally lasts for a short time and at a specific phase of the low frequency wave, it appears to be the result of a process that occurs because the plasma is unstable at a specific phase of the low frequency wave and $n=1$.

After formation, ion-acoustic waves steepen to create harmonics of the initial wave due to fluid nonlinearities [e.g., Davidson, 1972]. The steepening time scale can be estimated as $\lambda/2\pi\delta u$, where $\delta u \sim eE/2\pi f_h m_i$ is the amplitude of the ion bulk velocity fluctuations due to the electrostatic wave, and λ and f_h are the wavelength and wave frequency in the plasma rest frame. Using the observed amplitudes and assuming a reasonable phase speed of 200 km/sec for the ion-acoustic waves in the plasma frame, the steepening time scale of the TIAW high-frequency waves is a few seconds. A second nonlinear mechanism that produces harmonics of an initially monochromatic ion-acoustic wave, is ion trapping by the electrostatic wave [e.g. Davidson, 1972] and this process operates on a time scale of $\lambda/2\pi\delta u$, where $\delta u \sim (e\delta\phi/m_i)^{1/2}$ is the speed of the trapped ions, which is a few seconds as well. This widening produce waves at harmonics of the initial frequencies.

Figure 6 presents a rare example in which the high frequency wave of (6d) is continuous in time over the duration of the low frequency wave of (6e), so formation of harmonics should be observed. In panels (6a) and (6b), the 0-1000 Hz spectra of the electric field and density fluctuations show the fundamental wave at about 225 Hz and the first harmonic at about 450 Hz. Also, the next higher harmonic is barely visible in the electric field spectrum. In panel (6c) the same harmonic generation of the low frequency wave is observed in the 0-10 Hz spectral plot. Note that the steepening creates harmonics of the narrow band wave and does not broaden the spectrum of this wave. That the steepening is observed suggests that initially created waves last for more than the order of a second.

IIIi The low frequency wave in TIAW is a narrow band ion-acoustic wave.

Like the high frequency wave in TIAW, the low frequency wave is also nearly monochromatic. Figure (5a) shows that this is true for EX, and Figure (6c), which displays the power spectrum from 0 to 10 Hz, illustrates that the fundamental low frequency signal was a monotone at about 4 Hz.

A theory that might explain the generation of the low frequency ion-acoustic wave in the solar radial range of the present observations is based on the conservation of both the energy and the first invariant during the solar wind expansion [Kellogg, 2022]. This creates a hole in the ion distribution near zero velocity, which results in an instability that produces a low frequency electrostatic wave.

A different low frequency electrostatic wave mode may be generated if the plasma contains a mixture of electrons, protons and charged dust particles [Malaspina et al [2020]; Segwal and Sharma [2018]]. However, to create a dust wave at a frequency ~ 1 Hz requires a dust density orders-of-magnitude greater than that observed, so the low frequency TIAW must not be a dust wave.

IIj The <0.1 Hz electric field measured at times of the observed TIAW was in agreement with $-\mathbf{v}\times\mathbf{B}$, the motional electric field, which suggests that the instrument functioned nominally.

Figure 7 presents four hours of data that illustrate this fact. Panel (7a) of this figure gives the power spectrum of E_x which, on careful viewing, is seen to be composed of pulses of energy corresponding to the bursts of the high frequency component of the phase locked wave. Thus, triggered ion-acoustic waves were present through most of the interval. Panels (7b) and (7c) present the two components of the electric field and the components of $-\mathbf{v}\times\mathbf{B}$, the motional electric field, all of which are band pass filtered below 0.1 Hz. The agreement between the electric field measurements and $-\mathbf{v}\times\mathbf{B}$ shows that the very low frequency electric fields were well-measured. These very low frequency electric fields were produced by least-squares fitting the electric field to $-\mathbf{v}\times\mathbf{B}$. The two least-squares coefficients produced in this way are the effective antenna length of panel (7d) and the angular rotation of the X-Y plane in panel (7e) [Mozer et al, 2020a]. The reasonableness of these quantities as well as the excellent agreement between \mathbf{E} and $-\mathbf{v}\times\mathbf{B}$ show that the very low frequency electric field was well-measured, which suggests that there is no concern about the instrument operation during this time.

IIk The TIAW were not affected by variations of the plasma density or temperature, the solar wind speed, magnetic field orientation, etc., indicating that the measurement was not made in a wake or other effect that produced a spurious field.

To test the possibility that plasma parameter variations produced a spurious TIAW, as was the case for a different wave mode in Malaspina et al [2022], Figure 8 gives one example of the >400 Hz high frequency component of a triggered ion acoustic wave in panel (8a) that was continuously present while the magnetic field direction varied through about 75 degrees in panel (8b), T_e/T_i increased by about 40% in panel (8c), the solar wind speed decreased by about 25% in panel (8d) and the plasma density increased by about a factor of two in panel (8e). This is one example of many that suggests the TIAW were not due to a wake effect that occurred when the system geometry produced a changing wake around the spacecraft. It is also noted that the TIAW amplitude increased when T_e/T_i increased, which suggests that wave damping may have decreased due to an increased temperature ratio, as discussed in section IIg.

III The single ended potentials of the electric field measurement show that it performed normally.

Further evidence that the measured fields are physical comes from examination of the four antenna potentials, typical examples of which are presented in Figure 9. The four antenna voltages, filtered from 1-100 Hz, are presented in panels (9a), (9b), (9c), and (9d), while the same data, filtered above 100 Hz, are in the bottom four panels. At both the low and high frequencies, all four antennas produced good electric potentials with no indication that one or more of the potentials was perturbed by a wake or any other non-physical effect. Because this behaviour existed during all events, it represents strong evidence that the antennas performed nominally and that the triggered ion-acoustic waves are a real physical phenomenon.

IIIm The mechanism for the coupling of the two electrostatic waves in TIAW is not understood, although similar types of coupling are known.

The mechanism resulting in phase-locking between the high- and low-frequency electrostatic waves is not understood. Other observations have demonstrated that phase correlation between electrostatic spikes and whistler waves can occur due to the steepening process of the whistler wave electrostatic component under the resonance condition between electron-acoustic and whistler waves [Agapitov et al., 2018; Vasko et al., 2018; An et al., 2019]. The coupling between Langmuir and ion-acoustic waves has also been shown theoretically [Nishikawa et al, 1974].

Recent simulations showed that electrostatic fluctuations can be observed at a specific phase of an oblique whistler wave, since the drift between cold and hot electrons associated with the whistler wave results in a high-frequency electrostatic instability [Roytershteyn and Delzanno, 2021]. Following this idea, one may hypothesize that the phase-locking observed in triggered ion-acoustic waves is due to a current-driven instability producing high-frequency electrostatic waves at the specific phase of the low-frequency electrostatic wave. In this case, the phase-locking is observed because the high-frequency waves are at the phase where the plasma is unstable. The viability of this mechanism for triggered ion-acoustic waves deserves a separate study, while here we only point out that the ion-electron drift velocity associated with the low-frequency waves is negligible compared to the ion-acoustic speed and, thus, not likely to be unstable.

III SUMMARY

In summary, the above results show that the electric field instrument functioned normally (IIj and III), that it measured two electrostatic waves (IIb) that had the nearly same phase velocity (III) and that satisfied the requirements of electrostatic waves because the electric field and density fluctuations were 90 degrees out of phase (IIf), the electric field was parallel to the k-vector (IIc), and the phase velocity was consistent with that expected for an ion-acoustic wave (IId). These linked waves were found on most orbits between 20 and 25 solar radii in regions where $T_e/T_i > 1$ (due to a low ion temperature) such that ion Landau damping was small and they might survive for hours (IIg). The electric field and density fluctuations in the high frequency wave were nearly monochromatic (IIh). The low frequency wave was also narrow band with harmonics and it was likely an ion-acoustic wave and not a dust mode (IIi). Because the TIAW were found in conjunction with electron heating more than seven times in the 20-25 solar radius range and were

absent in the one example of no electron heating in this distance range, and because there was sufficient potential in the low frequency TIAW wave to heat the electrons (IIa), it is likely that the TIAW played a significant role in solar wind heating and in astrophysics.

The triggered ion-acoustic waves did not depend strongly on plasma parameters such as the ion temperature, the density, the magnetic field, or the solar wind speed (IIk). Why or how the high and low frequency components of the triggered ion-acoustic wave were coupled is not understood but similar phenomena have been found between other wave pairs (IIm). Thus, the evidence that the triggered ion-acoustic waves are a real physical phenomenon that is important to the solar wind physics is very strong, although a non-physical source cannot be completely ruled out. That it cannot be ruled out as an artifact is the case for almost any physical observation made in space.

IV ACKNOWLEDGEMENTS

This work was supported by NASA contracts NNN06AA01C and 80NSSC21K0581. The authors acknowledge the extraordinary contributions of the Parker Solar Probe spacecraft engineering team at the Applied Physics Laboratory at Johns Hopkins University. The FIELDS experiment on the Parker Solar Probe was designed and developed under NASA contract NNN06AA01C. Our sincere thanks to P. Harvey, K. Goetz, and M. Pulupa for managing the spacecraft commanding, data processing, and data analysis, which has become a heavy load thanks to the complexity of the instruments and the orbit. We also acknowledge the SWEAP team for providing plasma data. The work of I.V. was supported by National Science Foundation Grant No. 2026680. The work of J.V. was supported by NASA PSP-GI 80NSSC23K0208.

TABLE 1

PLASMA PARAMETERS AT 01:19:15 ON 06/01/2021

Magnetic field	200	nT
Density	1100	cm ⁻³
Ion temperature	20	eV
Core electron temperature	54	eV
Solar wind speed	190	km/sec
Solar wind v _X	-85	km/sec
Solar wind v _Y	-4	km/sec
Solar wind v _Z	-170	km/sec
Ion beta	0.2	
Proton Debye length	0.8	m
Alfven speed	100	Km/sec
Electron gyrofrequency	6000	Hz

VI REFERENCES

Agapitov O., Drake J. F., Vasko I., Mozer F. S., Artemyev A., Krasnoselskikh V., Angelopoulos V., Wygant J., Reeves G. D., “Nonlinear Electrostatic Steepening of Whistler Waves: The Guiding Factors and Dynamics in Inhomogeneous Systems”, *Geophysical Research Letters*, vol. 45, no. 5, pp. 2168–2176, 2018. doi:10.1002/2017GL076957.

An X., Li, J., Bortnik J., Decyk V., Kletzing C., and Hospodarsky G., “Unified View of Nonlinear Wave Structures Associated with Whistler-Mode Chorus”, *Physical Review Letters*, vol. 122, no. 4, 2019. doi:10.1103/PhysRevLett.122.045101.

Bale, S.D., Goetz, K., Harvey, P.R., Turin, P. Bonnell, J. W., Dudok de Wit, T., Ergun, R.E., MacDowall, R. J., Pulupa, M.; Andre, M., et al, “The Fields Instrument Suite for Solar Probe Plus”, *SSRv*, 204, 49 (2016)

Boldyrev, S., Forest, C., Egedal, J.,” Electron temperature of the solar wind”, *PNAS*, **117**, (2020)

Davidson, R.C., “Methods in nonlinear plasma theory”, eBook ISBN: 9780323153386, Elsevier, (1972)

Gurnett, D.A. and L. A. Frank, 1978, *J. Geophys. Res.*, **83**, 1

Gurnett, D. A. and Anderson, R. R., 1977, *Journal of Geophysical Research*, Volume 82, Issue 4, p. 632

Hull A. J., Larson, D.E., Wilber, M., Scudder, J.D., Mozer, F.S., Russell, C.T., and Bale, S.D. ., Large-amplitude electrostatic waves associated with magnetic ramp substructure at Earth's bow shock, *Geophysical Research Letters*, vol. 33, no. 15, doi:10.1029/2005GL025564. (2006)

Kasper, J. C., Abiad, R., Austin, G., Balat-Pichelin, M., Bale, S.D., Belcher, J.W., Berg, P., Bergner, H., Berthomier, M., Bookbinder, J., et al, Solar Wind Electrons Alphas and Protons (SWEAP) Investigation: Design of the Solar Wind and Coronal 171 Plasma Instrument Suite for Solar Probe Plus. *Space Sci. Rev.* 204, 131–186, DOI 10.1007/s11214-015-0206-3. (2016)

Kelley, M. C. and Mozer, F. S., A technique for making dispersion relation measurements of electrostatic waves, *Journal of Geophysical Research*, vol. 77, no. 34, pp. 6900–6903. doi:10.1029/JA077i034p06900 (1972).

Kellogg, P.J. “A fundamental instability for the solar wind”, *The Astrophysical Journal*, **925**, 2, (2022)

Kurth, W. S., Gurnett, D. A., and Scarf, F. L., High-resolution spectrograms of ion-acoustic waves in the solar wind, *Journal of Geophysical Research*, vol. 84, no. A7, pp. 3413–3413. doi:10.1029/JA084iA07p03413 (1979).

Livi, R., Larson, D.E., Kasper, J.C., Abiad, R., Case, A.W., Klein, K.G., Curtis, D.W., Dalton, G., Stevens, M., Korreck, K.E., *The Astrophysical Journal*, **938**, 138, doi:10.3847/1538-4357/ac93f5, (2022)

Malaspina, D.M., Szalay, J.R., Pokorný, P., Page, B., Bale, S.D., Bonnell, J.W., Dudok de Wit, T.D., Goetz, K., Goodrich, K., Harvey, P.R., “In Situ Observations of Interplanetary Dust Variability in the Inner Heliosphere”, *ApJ* 892 115, DOI 10.3847/1538-4357/ab799b (2020)

Malaspina, D.M., Tigik, S., Vaivads, A., “Evidence that interaction with the Spacecraft Plasma Wake Generates Plasma Waves Close to the Electron Cyclotron Frequency in the Near-Sun Solar Wind,” *The Astrophysical Journal Letters*, **936**, doi:10.3847/2041-8213/ac8c8f, (2022)

Mozer, F. S., Agapitov, O. V., Bale, S. D., Bonnell, J. W., Bowen, T. A., & Vasko, I., DC and low-frequency electric field measurements on the Parker Solar Probe. *Journal of Geophysical Research: Space Physics*, 125, e2020JA027980. <https://doi.org/10.1029/2020JA027980>, (2020a).

Mozer, F. S., Bonnell, J. W., Bowen, T. A., Schumm, G., and Vasko, I. Y., Large-amplitude, Wideband, Doppler-shifted, Ion-acoustic Waves Observed on the Parker Solar Probe, *The Astrophysical Journal*, vol. 901, no. 2. doi:10.3847/1538-4357/abafb4 (2020).

Mozer, F.S., Vasko, I.Y., and Verniero, J.L., “Triggered Ion-acoustic Waves in the Solar Wind”, *The Astrophysical Journal Letters*, 919:L2, 2021, <https://doi.org/10.3847/2041-8213/ac2259> (2021)

Mozer, F.S., Bale, S.D., Cattell, C.A., Halekas, J., Vasko, I.Y., Verniero, J.L., and Kellogg, P.J., “Core Electron Heating by Triggered Ion-acoustic Waves in the Solar Wind”, *The Astrophysical Journal Letters*, 927:L15, 2022a, <https://doi.org/10.3847/2041-8213/ac5520>

Mozer, F.S., Bale, S.D., Kellogg, P.J., Larson, D.E., Livi, R., and Romeo, O., “An Improved Technique for Measuring Plasma Density to High Frequencies on the Parker Solar Probe”, *The Astrophysical Journal*, 926:220, 2022b, <https://doi.org/10.3847/1538-4357/ac4f42>, (2022b)

Nishikawa, K., Hojo, H., and Mima, K., “Coupled Nonlinear Electron-Plasma and Ion-Acoustic Waves”, *Phys. Rev. Lett.*, **33**, 3, (1974)

Roytershteyn V. and Delzanno G. L., “Nonlinear coupling of whistler waves to oblique electrostatic turbulence enabled by cold plasma”, *Physics of Plasmas*, vol. 28, no. 4, 2021. doi:10.1063/5.0041838.

Segwal, K.R., and Sharma, S.C., “Current-Driven Low-Frequency Electrostatic Waves in a Collisional Strongly Coupled Magnetized Dusty Plasma”, *IEEE Transactions on plasma science*, **46**, (2018)

Vasko I. Y., Agapitov O., Mozer F. S., Bonnell J. W., Artemyev A. V., Krasnoselskikh V. V., Tong Y., “Electrostatic Steepening of Whistler Waves”, *Physical Review Letters*, vol. 120, no. 19, 2018. doi:10.1103/PhysRevLett.120.195101.

Vasko, I.Y., Mozer, F.S., Bale, S.D., and Artemyev, A.V., “Ion-Acoustic Waves in a Quasi-Perpendicular Earth's Bow Shock”, *Geophysical Research Letters*, vol. 49, no. 11, doi: 10.1029/2022GL098640. (2022)

Whittlesey, P.L., Larson, D.E., Kasper, J.C. Halekas, J., Abatcha, M., Abiad, R., Berthomier, M., Case, A.W., Chen, J., Curtis, D.W., et al, “The Solar Probe ANalyzers—Electrons on the Parker Solar Probe” ,*The Astrophysical Journal Supplement Series*, 246:74 (14pp), February <https://doi.org/10.3847/1538-4365/ab7370> © 2020. (2020)

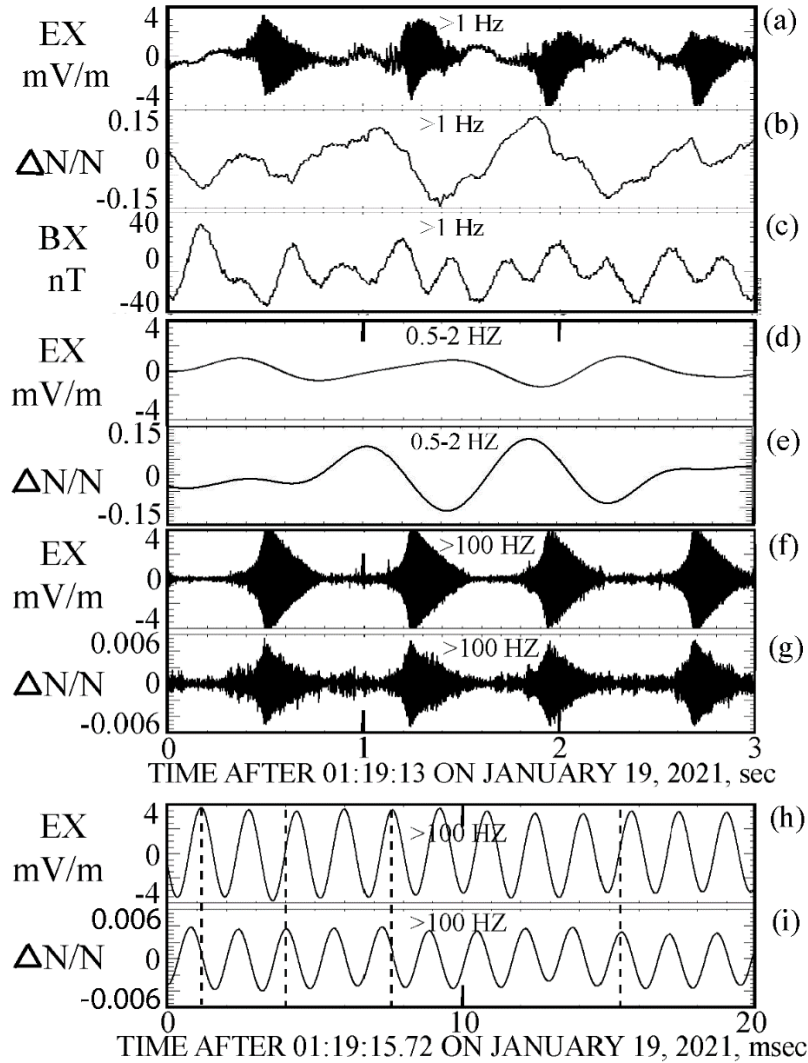


Figure 1. Four pairs of measurements of EX and density fluctuations. The pair (1a), (1b) are high pass filtered at 1 Hz to display the phase locked low and high frequency signatures of the triggered ion-acoustic wave. Panels (1d) and (1e) are bandpass filtered at 0.5-2 Hz to display the low frequency components of the wave. The pair (1f), (1g) are high pass filtered at 100 Hz to show the high frequency components. The pair (1h), (1i) provide >100 Hz filtered data over a short time interval to illustrate the pure sine wave nature of the high frequency component. Figure (1c) displays the magnetic field which had 10 cycles during the three seconds of interest as compared to the 4 cycles of the other components. Figure (1c) is an electromagnetic wave having no component at the frequency of the electrostatic triggered ion acoustic waves

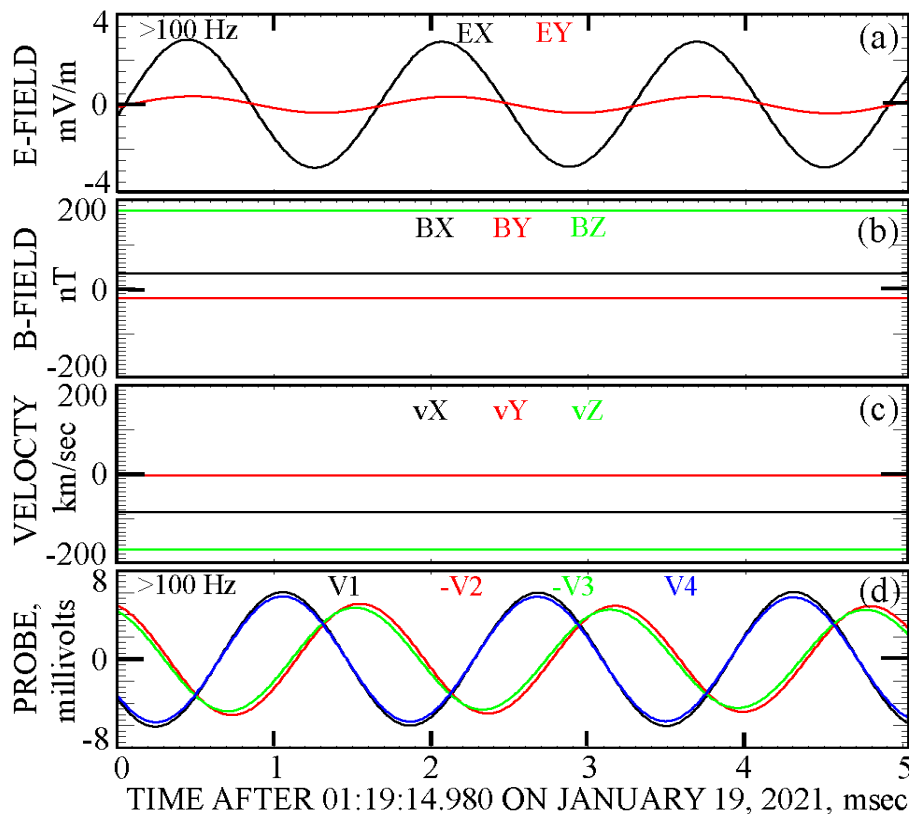


Figure 2. The >100 Hz EX and EY of the TIAW in panel (2a), the 200 nT background magnetic field vectors in the X-Y-Z frame in panel (2b), the 200 km/sec solar wind velocity in panel (2c), and the timing of the signals received by the four antennas for the event of Figure 1 in panel (2d). The cadences of the electric and magnetic field measurements are about 600 samples/second. The magnetic field and velocity data of panels (2b) and (2c) are unfiltered, and they are straight lines because their data rates of ~ 1 Hz are not enough to show variations on the five millisecond time scale of this figure.

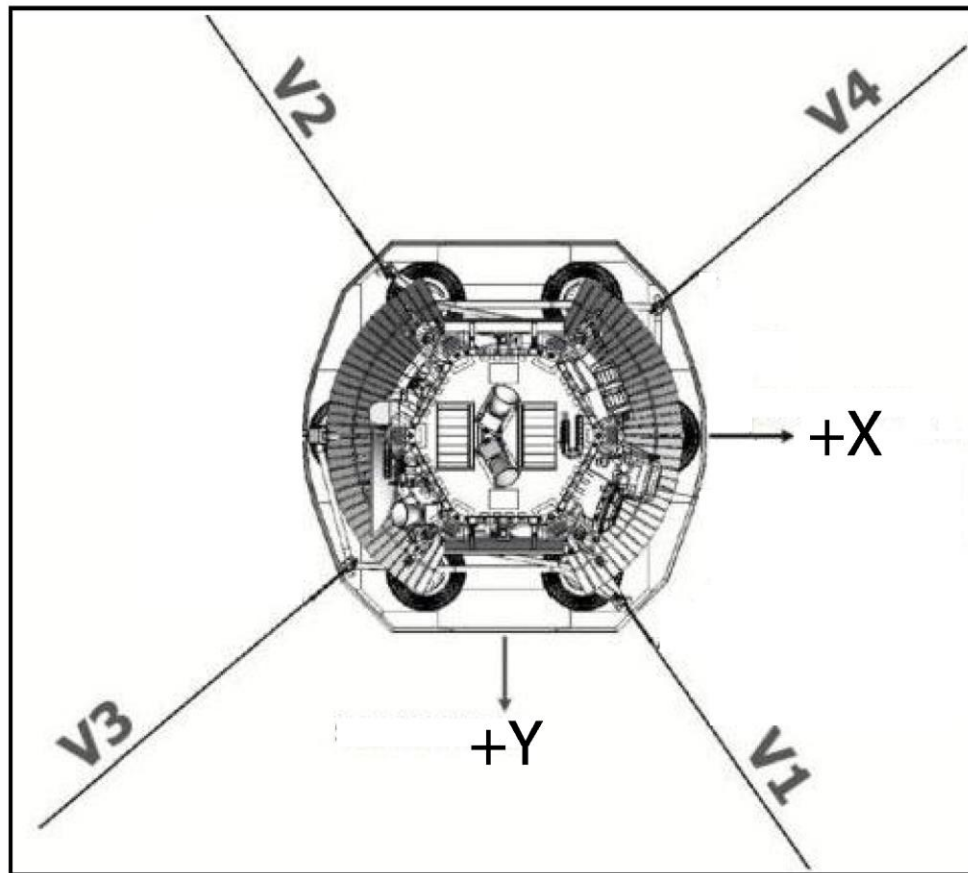


Figure 3. Orientation of the electric field antennas with respect to the X and Y axes.

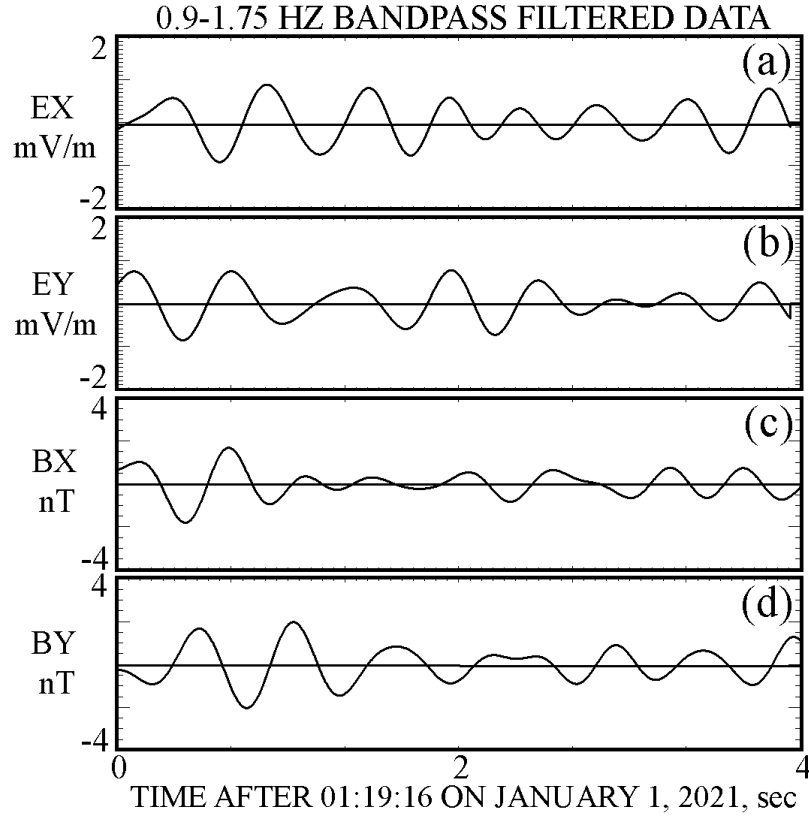


Figure 4. Two components of the electric field in panels (4a) and (4b) and the magnetic field in panels (4c) and (4d). Because EX is nearly a pure sine wave, the electrostatic E-field in this component greatly exceeded the electromagnetic E-field. By contrast EY correlated with BX to suggest that the electrostatic E-field was smaller than the electromagnetic E-field in this component.

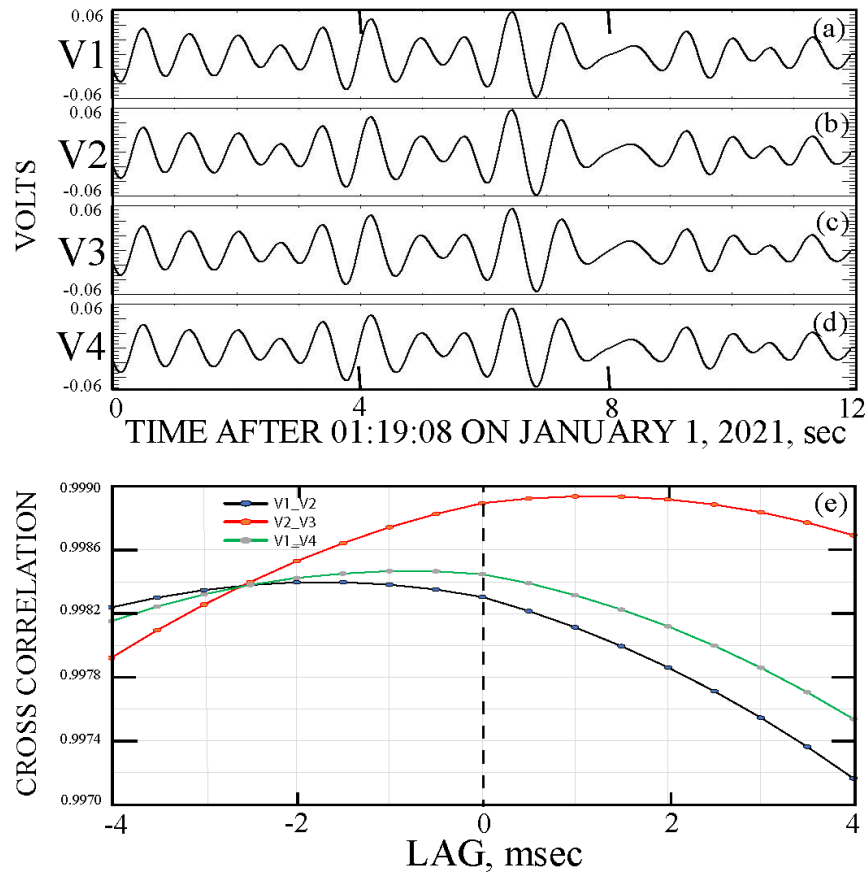


Figure 5. The four antenna potentials in panels (5a), (5b), (5c), and (5d), covering the time interval of Figures 1 and 2, and band pass filtered between 0.95 and 1.75 Hz. The phase lags between antenna pairs in panel (5e) give the times required for the low frequency wave to travel between antenna pairs and lead to the conclusion that, in the X-Y plasma frame, the low frequency wave's phase velocity has the same magnitude and direction as does the high frequency wave.

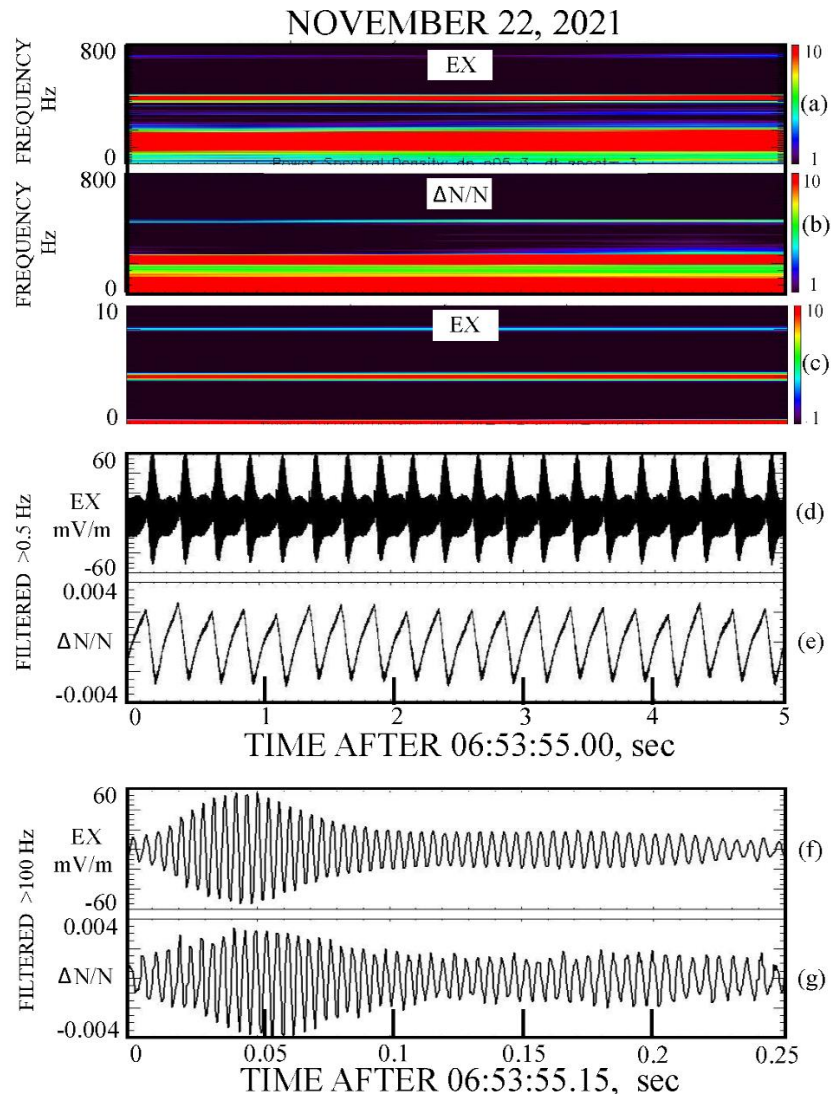


Figure 6. Illustration of a triggered ion-acoustic wave whose high frequency component appeared continuously during the low frequency component, as seen in panels (6c) and (6d), which present the >0.5 Hz filtered EX electric field and the density fluctuations. Panels (6e) and (6f) present 0.25 second segments of the >100 Hz fields and density fluctuations in order to illustrate the pure sine wave nature of the signals that persist throughout the low frequency signal. Because these high frequency signals are present continuously, it is expected that they should steepen to produce harmonics of the fundamental frequency. Panels (6a) and (6b) present the 0-1000 Hz spectra of the electric field and density fluctuations that show both the presence of the fundamental signals at about 225 Hz, and also the first harmonics at about 450 Hz. In the electric field spectrum, there is also a weak signature at the next harmonic. Panel (6c) presents the 0-10 Hz spectrum of the electric field which shows the narrow band low frequency wave at 4 Hz and its first harmonic at 8 Hz.

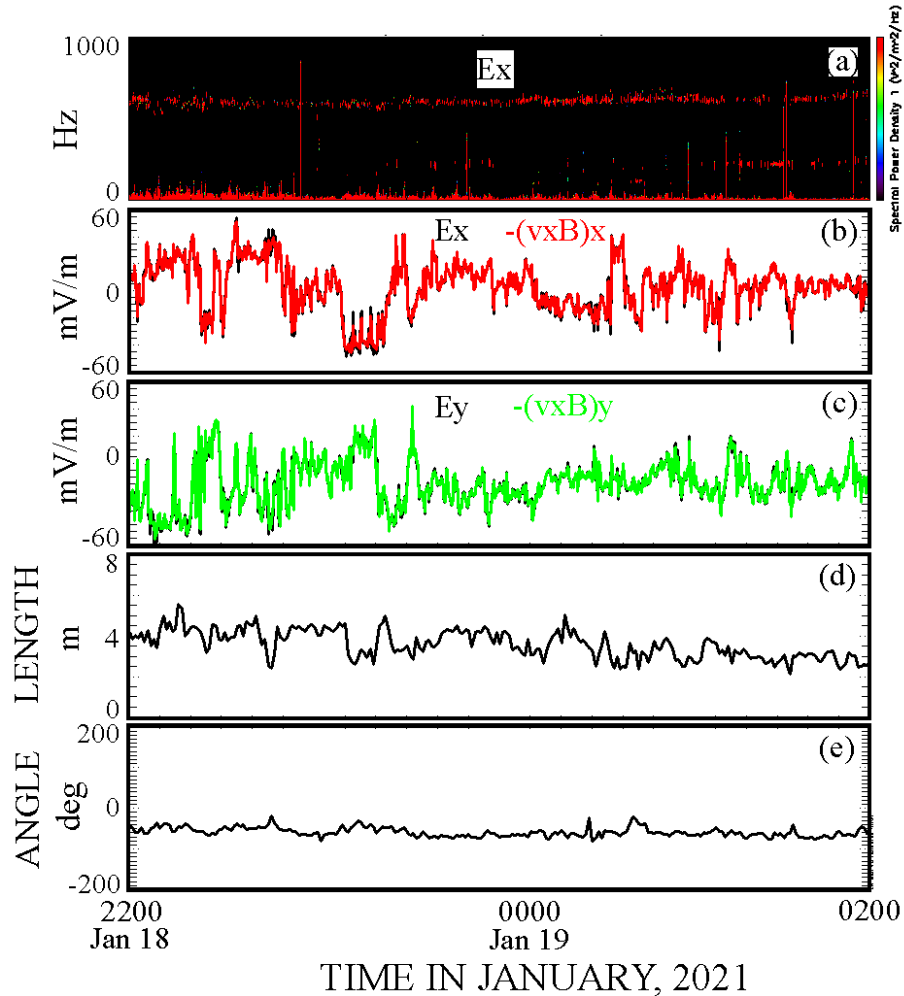


Figure 7. A four hour interval illustrating the accuracy of the <0.1 Hz electric field measurements. Panel (7a) gives the electric field spectrum which, on close examination, consists of a series of red dots showing that the 600 Hz pure sine wave occurred in triggered bursts through the interval. Panel (7b) gives the dc and low frequency X-component of the electric field and the X-component of $-\mathbf{v}\times\mathbf{B}$. Panel (7c) provides the same data for the Y-components. The agreement between \mathbf{E} and $-\mathbf{v}\times\mathbf{B}$ shows that the instrument functioned normally during this interval. The electric field is obtained from a least-squares fit described in Mozer et al [2020a], and the two least-squares coefficients are shown in panels (7d) and (7e).

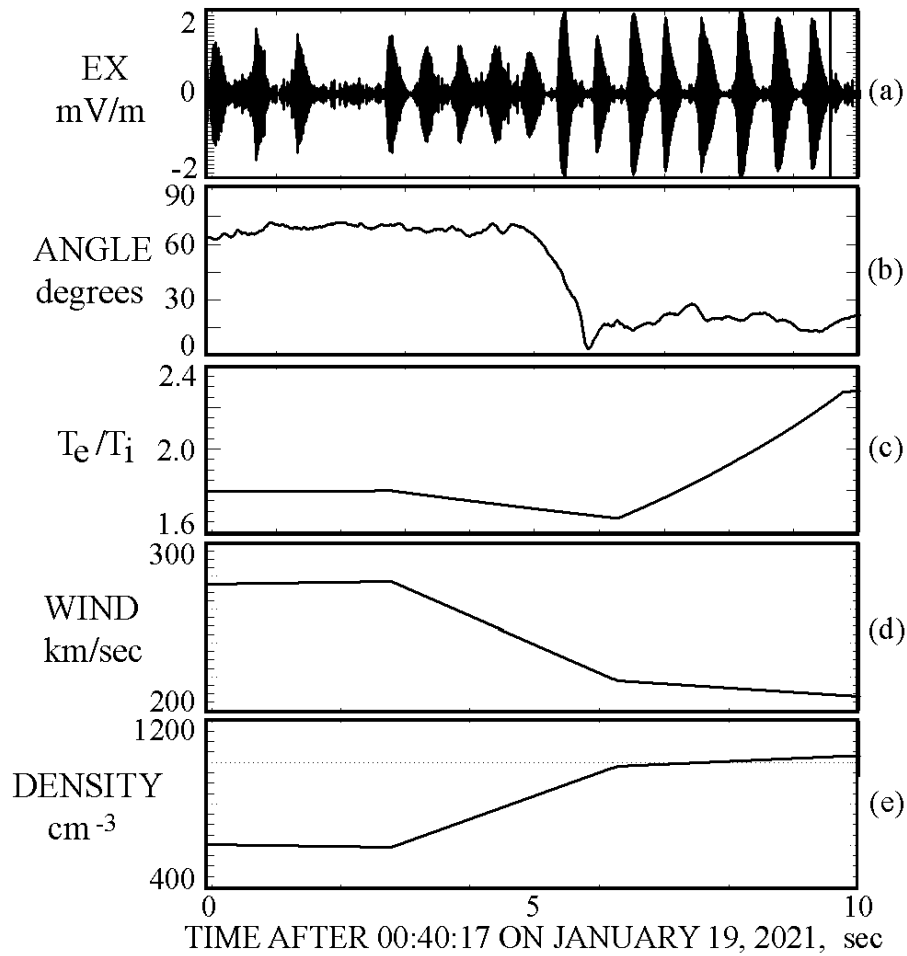


Figure 8. A 10 second period during the events of Figure 7 in which the high frequency component of a triggered ion acoustic wave was continuously present in panel (8a) while the magnetic field direction varied through about 75 degrees in panel (8b), T_e/T_i increased by about 40% in panel (8c), the solar wind speed decreased by about 25% in panel (8d) and the plasma density increased by about a factor of two in panel (8e). This is one of many examples that suggest the TIAW were not due to a wake effect that occurred when the system geometry might have produced wakes around the spacecraft. It is also noted that the TIAW amplitude increased when T_e/T_i increased, which suggests that wave damping may have decreased at this time due to an increased temperature ratio.

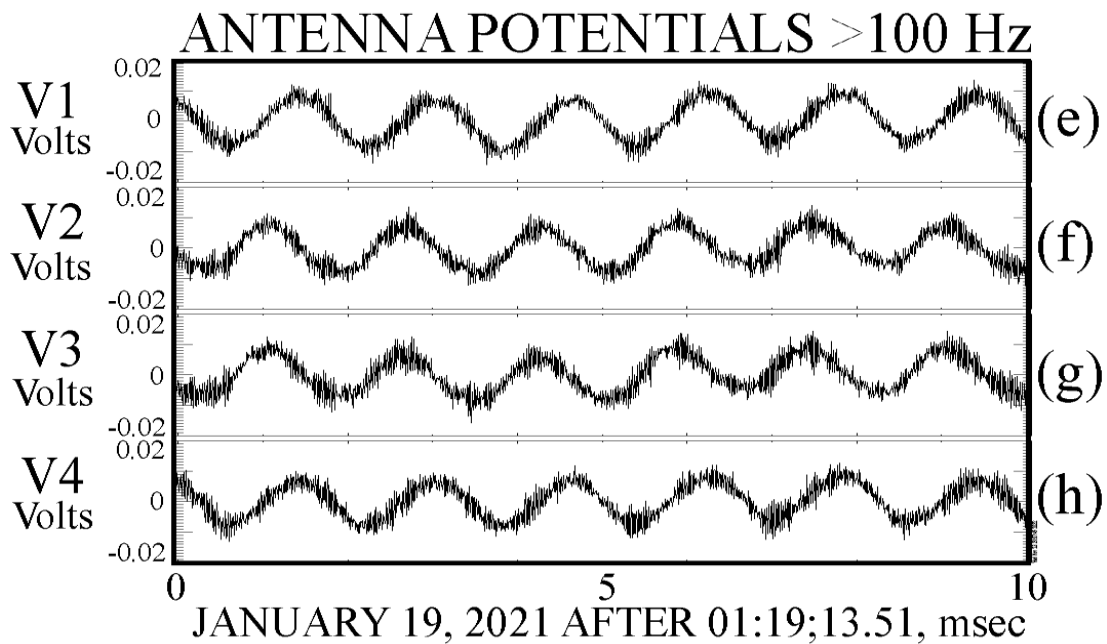
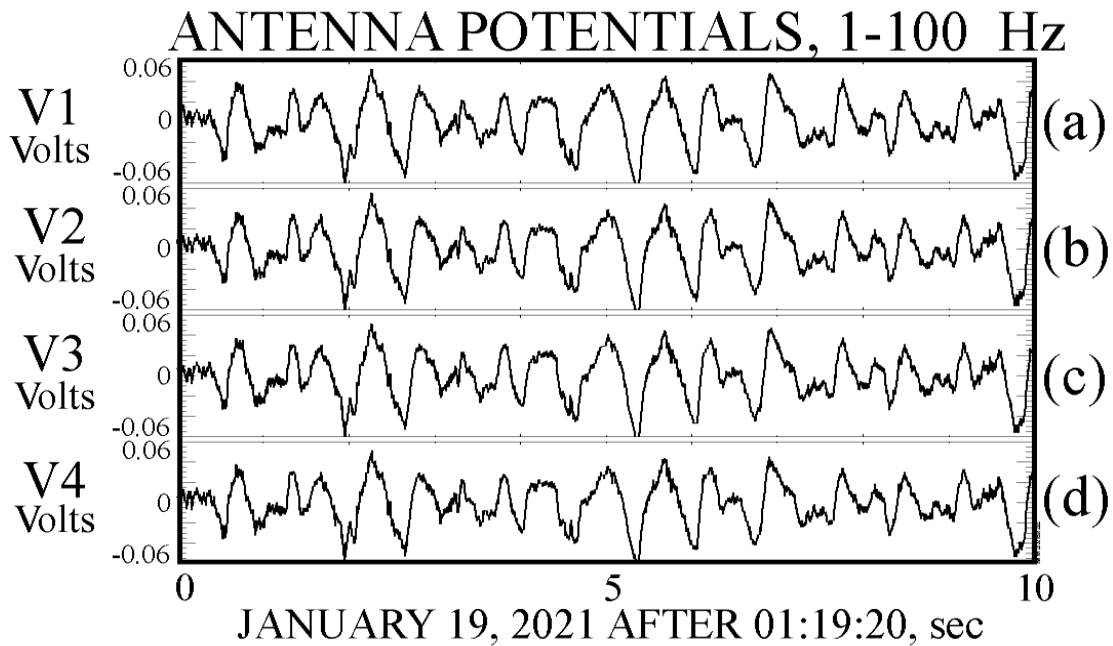


Figure 9. Panels (9a) through (9d) give the four antenna potentials (V1, V2, V3, and V4) filtered from 1 to 100 Hz. Panels (9e) through (9h) provide the same data after being high pass filtered above 100 Hz. In both cases, all of the antennas operated normally with no indication of one or more of them being affected by a wake or other non-physical process. This provides strong evidence that the electric field instrument performed normally and that the observed waves were physical and not an artifact resulting from a wake or detector malfunction.